

# Quantum simulation of a class of highly-oscillatory transport equations via Schrödingerisation

Anjiao Gu<sup>1,2</sup> and Shi Jin<sup>\*1,2,3</sup>

<sup>1</sup>*School of Mathematical Sciences, Shanghai Jiao Tong University, Shanghai 200240, China*

<sup>2</sup>*Institute of Natural Sciences, Shanghai Jiao Tong University, Shanghai 200240, China*

<sup>3</sup>*Ministry of Education Key Laboratory in Scientific and Engineering Computing, Shanghai 200240, China*

## Abstract

In this paper, we present quantum algorithms for a class of highly-oscillatory transport equations, which arise in semiclassical computation of surface hopping problems and other related non-adiabatic quantum dynamics, based on the Born-Oppenheimer approximation. Our method relies on the classical nonlinear geometric optics method, and the recently developed Schrödingerisation approach for quantum simulation of partial differential equations. The Schrödingerisation technique can transform any linear ordinary and partial differential equations into Hamiltonian systems evolving under unitary dynamics, via a warped phase transformation that maps these equations to one higher dimension. We study possible paths for better recoveries of the solution to the original problem by shifting the bad eigenvalues in the Schrödingerized system. Our method ensures the uniform error estimates *independent* of the wave length, thus allowing numerical accuracy, in maximum norm, even without numerically resolving the physical oscillations. Various numerical experiments are performed to demonstrate the validity of this approach.

**Keywords:** Quantum simulation, Schrödingerisation, highly oscillatory transport PDEs, nonlinear geometric optics method

## 1 Introduction

As the classical computer is increasingly closer to its physical limit [19], a potentially effective path to the future computing platform is quantum computing [18] which are currently under rapid development. Compared with classical methods, quantum algorithms have already been shown to have certain advantages in a number of problems [12, 14, 32]. For instance, the HHL algorithm proposed by Harrow, Hassidim and Lloyd in [20] can realize exponential acceleration when solving systems of linear

---

\*Corresponding author: shijin-m@sjtu.edu.cn.

equations under several conditions. Such successful cases motivate one to extend the high-cost classical algorithms of important scientific problems to quantum algorithms [33, 13, 34]. In particular, quantum algorithms for solving ordinary or partial differential equations have received extensive recent attention [3, 29, 15, 10, 8, 9, 26].

In this paper, we concentrate on a family of transport equations in which the phase oscillations depend on both time and space as follows

$$\begin{aligned} \partial_t u + \sum_{k=1}^d A_k(x) \partial_{x_k} u &= \frac{iE(t, x)}{\varepsilon} Du + Cu, \\ u(0, x) &= f_0(x, \beta/\varepsilon), \quad x \in \Omega \subset \mathbb{R}^d, \end{aligned}$$

where  $u(t, x) \in \mathbb{C}^n$ ,  $A_k$  and  $D$  are  $n \times n$  real symmetric matrices,  $C \in \mathbb{R}^{n \times n}$ . A number of semiclassical models in quantum dynamics can be written in this form, such as surface hopping [7], graphene [31], quantum dynamics in periodic lattice [30], etc. Solving such systems is computationally daunting since 1) often the dimension is high ( $d \gg 1$ ), and 2) one needs to numerically resolve the small wave lengths which are of  $O(\varepsilon)$  [28, 17]. The nonlinear geometric optics (NGO) based method, developed in [11] for above problems, uses a nonlinear eometric optics ansatz which builds the oscillatory phase as an independent variable, and a suitably chosen initial data derived from the Chapman-Enskog expansion, guarantee that one can use mesh size and time step *independent of*  $\varepsilon$ . However, the curse-of-dimensionality remains the bottleneck for classical computation. This motivates us to consider quantum algorithms for this problem, which has no curse-of-dimensionality due to the use of qubits, since in general one just needs  $n = \log_2 d$  qubits for  $d$ -dimensional problems.

Our main tool for quantum simulation is a new method called Schrödingerisation which have been recently proposed for solving general linear ordinary and partial differential equations [26, 27]. This technique can convert non-unitary dynamics (linear differential equations) to unitary dynamics (Schrödinger type equations) by a warped phase transformation that just maps the system to one higher dimension, followed by a Fourier transform. The original variable can be recovered via integration on or pointwise evaluation of the extra variable. This method works for both qubits [26, 27] and continuous-variable frameworks [22], open quantum systems with artificial boundary conditions [23], physical boundary or interface conditions [21], etc. and problems with time-dependent coefficientis [5, 1, 2, 16, 6].

The outline of this paper is as follows. In Section 2, we give a brief review of the Schrödingerisation method. Then, based on the nonlinear geometric optics approach, we apply the Schrödingerisation algorithm together with spectral and finite difference discretisations on the equations, for one dimensional scalar equations in Section 3. We provide numerical results for problems of different settings. In Section 4, we extend the new approach to a class of PDE system which is the semi-classical approximation of surface hopping problem [7], and show the effectiveness of our method for such highly-oscillatory transport problems by presenting some typical numerical examples. Finally, we conclude this paper in Section 5.

Throughout this paper, we consider the problems in a finite time interval, i.e.  $T = \mathcal{O}(1)$ . For arbitrary vector  $\mathbf{a} = (a_0, a_1, \dots, a_{n-1})^T$ , we use the notation  $\text{diag}\{\mathbf{a}\} = \text{diag}[a_0, a_1, \dots, a_{n-1}]$  to denote the matrix  $\sum_j a_j |j\rangle \langle j|$ .

## 2 Description of Schrödingerisation

We begin with a brief presentation of the Schrödingerisation method. It was first proposed in [26, 27] and can be applied to quantum simulation for general linear dynamical systems, including both systems of ODEs and PDEs:

$$\frac{d\mathbf{u}}{dt} = A\mathbf{u} + \mathbf{b}, \quad \mathbf{u}(0) = \mathbf{u}_0, \quad (1)$$

where  $\mathbf{u}, \mathbf{b} \in \mathbb{C}^n$  and  $A \in \mathbb{C}^{n \times n}$  is a linear (for ODEs) or linear differential (for PDEs) operator. We firstly present the Schrödingerisation method for time-independent  $A$  and  $\mathbf{b}$ . First, (1) can be rewritten as a homogeneous system:

$$\frac{d\tilde{\mathbf{u}}}{dt} = \tilde{A}\tilde{\mathbf{u}}, \quad \tilde{\mathbf{u}} = \begin{bmatrix} \mathbf{u} \\ \mathbf{r} \end{bmatrix}, \quad \tilde{A} = \begin{bmatrix} A & B \\ \mathbf{0} & \mathbf{0} \end{bmatrix}, \quad \tilde{\mathbf{u}}(0) = \begin{bmatrix} \mathbf{u}_0 \\ \mathbf{r}_0 \end{bmatrix}, \quad (2)$$

where  $B = \text{diag}\{\mathbf{b}\}$  and  $\mathbf{r}_0 = \sum_j |j\rangle$ .  $\tilde{A}$  can be further decomposed into a Hermitian term and an anti-Hermitian one:

$$\tilde{A} = H_1 + iH_2, \quad H_1 = \frac{\tilde{A} + \tilde{A}^\dagger}{2}, \quad H_2 = \frac{\tilde{A} - \tilde{A}^\dagger}{2i}. \quad (3)$$

Using the warped phase transformation  $\mathbf{v}(t, p) = e^{-p}\tilde{\mathbf{u}}(t)$  for  $p > 0$  and properly extending the initial data to  $p < 0$ , equation (2) are then transferred to linear convection equations:

$$\frac{d\mathbf{v}}{dt} = -H_1\partial_p\mathbf{v} + iH_2\mathbf{v}, \quad \mathbf{v}(0) = \xi(p)\tilde{\mathbf{u}}(0). \quad (4)$$

Here, the smoothness of  $\xi(p)$  has an impact on the convergence rate of the numerical method. For instance, if we use  $\xi(p) = e^{-|p|}$ , it implies a first-order accuracy on the spatial discretization due to the regularity in  $p$  of the initial condition. And if one uses a smoother initial value of  $\mathbf{v}(0)$  with

$$\xi(p) = \begin{cases} (-3 + 3e^{-1})p^3 + (-5 + 4e^{-1})p^2 - p + 1, & p \in (-1, 0), \\ e^{-|p|}, & \text{otherwise,} \end{cases} \quad (5)$$

it gives a second-order accuracy [24, 25]. Higher order accuracy can also be achieved by requiring smoother  $\xi(p)$ , see [25].

### 2.1 The discrete Fourier transform for Schrödingerisation

We discuss the discrete Fourier transformation (DFT) on  $p$  in this section. We use the uniform mesh size  $\Delta p = (R - L)/M$  for  $M = 2N$  and denote the grid points as

$$p_j = L + j\Delta p, \quad j = 0, 1, \dots, M.$$

The basis functions are chosen as

$$\phi_l(x) = e^{i\mu_l(x-L)}, \quad \mu_l = \frac{2\pi(l-N)}{R-L}, \quad l \in [M].$$

Here  $[M] = \{0, 1, \dots, M-1\}$ . Then we can define

$$\Phi_p = (\phi_{jl})_{M \times M} = (\phi_l(p_j))_{M \times M}, \quad D_p = \text{diag}\{\mu_0, \dots, \mu_{M-1}\}.$$

After the transformation on  $p$ , equation (4) is transferred to

$$i \frac{d\mathbf{w}}{dt} = (H_1 \otimes P_p - H_2 \otimes I_{M_p})\mathbf{w},$$

where  $\mathbf{w} = \sum_{j,k} v_j(t, p_k) |j\rangle |k\rangle$  and  $P_p = \Phi_p D_p (\Phi_p)^{-1} = P_p^\dagger$ . By a change of variables  $\tilde{\mathbf{w}} = (I_{M_x} \otimes (\Phi_p)^{-1})\mathbf{w}$ , one can get a "Schrödingerized" system:

$$i \frac{d\tilde{\mathbf{w}}}{dt} = (H_1 \otimes D_p - H_2 \otimes I_{M_p})\tilde{\mathbf{w}} =: H\tilde{\mathbf{w}}. \quad (6)$$

In practical calculation, the Hamiltonian  $H$  is usually sparse, and has the following properties

$$s(H) = \mathcal{O}(s(\tilde{A})), \quad \|H\|_{\max} \leq \|H_1\|_{\max}/\Delta p + \|H_2\|_{\max},$$

where  $s(H)$  is the sparsity (maximum number of nonzero entries in each row and column) of the matrix  $H$  and  $\|H\|_{\max}$  is its max-norm (value of largest entry in absolute value). For general sparse Hamiltonian simulation, a quantum algorithm with a nearly optimal dependence on all parameters can be found in [4], with complexity given by the next lemma.

**Lemma 2.1.** [27] *An  $s$ -sparse Hamiltonian  $H$  acting on  $m_H$  qubits can be simulated within error  $\delta$  with*

$$\mathcal{O}(\tau \log(\tau/\delta)/(\log \log(\tau/\delta)))$$

*queries and*

$$\mathcal{O}\left(\tau[m_H + \log_{2.5}(\tau/\delta)] \frac{\log(\tau/\delta)}{\log \log(\tau/\delta)}\right)$$

*additional 2-qubits gates, where  $\tau = s\|H\|_{\max}T$ , and  $T$  is the stopping time.*

## 2.2 Recovery of the solution

If all eigenvalues of  $H_1$  are negative, the convection term of (4) corresponds to a wave moving from the right to the left, thus it does not need to impose a boundary condition for  $\mathbf{v}$  at  $p = 0$ . For the general case, i.e. if  $H_1$  has non-negative eigenvalues, one uses the following Theorem to recover the original solution.

**Theorem 2.2.** [24] *Assume the eigenvalues of  $H_1$  in (3) satisfy*

$$\lambda_1(H_1) \leq \lambda_2(H_1) \leq \dots \leq \lambda_n(H_1),$$

*then solution  $\tilde{\mathbf{u}}(T)$  can be restored by*

$$\tilde{\mathbf{u}} = e^{p_k} \mathbf{v}(p_k), \quad \text{or} \quad \tilde{\mathbf{u}} = e^{p_k} \int_{p_k}^{\infty} \mathbf{v} dp,$$

*where  $p_k \geq p_\star = \max\{\lambda_n(H_1)T, 0\}$ .*

The above Theorem means that we have to use qubits  $|p_k\rangle$  satisfying  $p_k \geq \lambda_n(H_1)T$  to recover the original variables for systems that contain unstable modes. On the other hand, we can further give the following corollary.

**Corollary 1.** *For the homogeneous system (2), we introduce the following initial-value problem:*

$$\frac{d\tilde{\mathbf{u}}^\lambda}{dt} = (H_1 - \lambda_0 I_{2n} + iH_2)\tilde{\mathbf{u}}^\lambda, \quad \tilde{\mathbf{u}}^\lambda(0) = \tilde{\mathbf{u}}(0). \quad (7)$$

where  $\lambda_0 \in \mathbb{R}$ . Then, by denoting  $\mathbf{v}^\lambda = \xi(p)\tilde{\mathbf{u}}^\lambda$  we can restore the solution  $\tilde{\mathbf{u}}^\lambda$  by

$$\tilde{\mathbf{u}}^\lambda = e^{p_k} \mathbf{v}^\lambda(p_k), \quad \text{or} \quad \tilde{\mathbf{u}}^\lambda = e^{p_k} \int_{p_k}^{\infty} \mathbf{v}^\lambda dp \quad (8)$$

where  $p_k \geq p_\star = \max\{(\lambda_n(H_1) - \lambda_0)T, 0\}$ . And  $\tilde{\mathbf{u}}(T)$  can be recovered by  $e^{\lambda_0 T} \tilde{\mathbf{u}}^\lambda(T)$ .

The above corollary gives us the freedom to shift the eigenvalues of  $H_1$  for changing the  $p_\star$  in Theorem 2.2. For instance, the new Hermite part  $H_1 - \lambda_0 I_{2n}$  only has non-positive eigenvalues when  $\lambda_0 \geq \lambda_n(H_1)$ . In this situation, it has  $p_\star = 0$ . However, changing the eigenvalues may not always brings good results. Concretely, by using the error estimate in [24], it leads to the following theorem.

**Theorem 2.3.** *Assume that the assumptions in Theorem 2.2 hold and  $\mathbf{v}_h^\lambda$  is computed by (6). Let  $R = -L \geq \max\{|\lambda_n(H_1) - \lambda_0|, |\lambda_1(H_1) - \lambda_0|\}T$ . Then, the error estimate for  $\mathbf{v}_h^\lambda$  is*

$$\|\tilde{\mathbf{v}}_h^\lambda - \tilde{\mathbf{v}}^\lambda\|_{L^2} \leq C \left( \Delta p^k + \sqrt{\frac{|\lambda_1(H_1) - \lambda_0|^2 T}{\Delta p}} e^{-\lambda_1(H_1)T + \lambda_0 T - R} \right) (\|\tilde{\mathbf{u}}(0)\| + \|\mathbf{v}^\lambda\|_{H^1}),$$

where  $C$  is a positive constant independent of mesh size and  $\mathbf{v}^\lambda \in H^k$ .

With this theorem, we can select an appropriate  $\lambda_0$  based on the actual situation to seek a better recovery. The followings are two illustrations.

**Example 2.1.**

- If  $\lambda_n(H_1) > 0$  and the error in the exponential part does not account for the majority, we can use  $\lambda_0 \in [0, \lambda_n(H_1)]$  satisfying

$$\Delta p^k \geq \sqrt{\frac{|\lambda_1(H_1) - \lambda_0|^2 T}{\Delta p}} e^{-\lambda_1(H_1)T + \lambda_0 T - R} \quad (9)$$

to get a smaller  $p_k$  for recovery without increasing the error.

- If  $\lambda_n(H_1) < 0$  and the error in the exponential part is the major one, we can choose  $\lambda_0 \in [\lambda_n(H_1), 0]$  satisfying (9) for achieving more accurate solutions.

It can be observed that the choice of  $\lambda_0$  will influence the region of  $p$ . Thus, one can also adopt a  $\lambda_0$  which is close to  $\frac{\lambda_1(H_1) + \lambda_n(H_1)}{2}$  to release  $R$ .

For the quantum state, one can directly employ a measurement on the  $p$ -register. After performing Hamiltonian simulation to implement the unitary operator  $e^{-iHT}$

on initial state  $|\tilde{\psi}(0)\rangle = \frac{\tilde{\mathbf{w}}(0)}{\|\tilde{\mathbf{w}}(0)\|}$ , we will get the state  $|\tilde{\psi}(T)\rangle$ . One can first apply the quantum Fourier transform (QFT) on the resulting state to retrieve  $|\psi(T)\rangle$ . By choosing an appropriate  $p_k \geq p_*$  to apply quantum measurement  $I_{M_x} \otimes |p_k\rangle\langle p_k|$  on  $|\psi(T)\rangle$ , then the state are collapsed to

$$|\psi_k(T)\rangle \approx \frac{1}{\mathcal{N}} \left( \sum_j v_j(T, p_k) |j\rangle \right) \otimes |k\rangle, \quad \mathcal{N} = \left( \sum_j |v_j(T, p_k)|^2 \right)^{1/2}$$

with probability  $P_r(T, p_k) = \frac{\|\mathbf{v}(T, p_k)\|^2}{\sum_l \|\mathbf{v}(T, p_l)\|^2}$ . Moreover, a direct computation gives

$$P_r(T, p \geq p_*) = \frac{1}{2} \frac{\|e^{-p_*} \tilde{\mathbf{u}}(T)\|^2}{\|\tilde{\mathbf{u}}(0)\|^2} + \mathcal{O}(\Delta p).$$

### 2.3 Application to non-autonomous ordinary differential equations

For the time-dependent Hamiltonian  $H$  in (6), we can adopt the method proposed in [6]. By adding a new variable  $s \in \mathbb{R}$ , (6) is then transformed to an autonomous equation

$$\frac{\partial \mathbf{z}}{\partial t} = -\frac{\partial \mathbf{z}}{\partial s} - iH(s)\mathbf{z}, \quad \mathbf{z}(0, s) = \delta(s)\tilde{\mathbf{w}}(0),$$

where  $\delta(s)$  is the Dirac function. By truncating the  $s$ -region to  $[L', R']$ , we can define the DFT matrices corresponding to the  $s$  variable similar to that of  $p$ . After the discrete Fourier spectral discretization on  $s$ , it yields

$$i \frac{d\tilde{\mathbf{z}}}{dt} = (D_s \otimes I + I_{M_s} \otimes H)\tilde{\mathbf{z}}, \quad \tilde{\mathbf{z}}(0) = (\Phi_s^{-1} \otimes I)(\boldsymbol{\delta}_s \otimes \tilde{\mathbf{w}}(0)),$$

where  $I = I_{2n} \otimes I_{M_p}$ ,  $\boldsymbol{\delta}_s = \sum_j \zeta_\omega(s_j) |j\rangle$  and  $\zeta_\omega$  is the regularizing function of  $\delta$ . For  $x \in \mathbb{R}$ , it usually takes  $\zeta_\omega(x) = \frac{1}{\omega} \zeta(\frac{x}{\omega})$  with  $\zeta(x) = 1 - |x|$  or  $\zeta(x) = 1/2(1 + \cos(\pi x))$  whose support is  $[-1, 1]$ .

## 3 One dimensional scalar equations

We first review the geometrical optics (GO) based method introduced in [11] for the deterministic one dimensional scalar equation,

$$\partial_t u + c(x)\partial_x u + \lambda u = \frac{ia(x)}{\varepsilon} u, \quad u(0, x) = u_0(x), \quad (10)$$

where  $u(t, x) \in \mathbb{C}$ ,  $x \in \Omega_x$ ,  $t \geq 0$ , and  $\lambda$  is a complex constant. The functions  $u_0$ ,  $a$  and  $c$  are given while periodic boundary conditions are considered in space. Furthermore, function  $a$  satisfies  $a(x) \geq a_0 > 0$ ,  $\forall x \in \Omega_x$ . We will also allow the initial data to be oscillatory

$$u_0(x) = f_0(x, \beta(x)/\varepsilon) \equiv f_0(x, \tau) \quad \text{with} \quad \tau = \frac{\beta(x)}{\varepsilon},$$

where  $\beta$  is given and  $f_0$  is assumed to be periodic w.r.t. variable  $\tau$ . Then we expand the initial data with regard to the periodic variable  $\tau$ :

$$u_0(x) = \sum_{k \in \mathbb{Z}} f_k(x) e^{ik\beta(x)/\varepsilon} \equiv \sum_{k \in \mathbb{Z}} u_k(t, x),$$

and after applying to (10) one can get the following equations

$$\partial_t u_k + c(x) \partial_x u_k + \lambda u_k = \frac{ia(x)}{\varepsilon} u_k, \quad u_k(0, x) = f_k(x) e^{ik\beta(x)/\varepsilon}. \quad (11)$$

Indeed the linearity of equation (10) allows the use of the superposition principle which means the solution can be recovered by  $u(t, x) = \sum_k u_k(t, x)$ . Then we apply the standard Geometric Optics (GO) method by injecting the ansatz

$$u_k(t, x) = \alpha_k(t, x) e^{iS_k(t, x)/\varepsilon} \quad (12)$$

into (11) to get

$$\partial_t \alpha_k + c(x) \partial_x \alpha_k + \lambda \alpha_k + \frac{i}{\varepsilon} [\partial_t S_k + c(x) \partial_x S_k] \alpha_k = \frac{ia(x)}{\varepsilon} \alpha_k.$$

To remove the terms in  $1/\varepsilon$ , one can impose the following equations on  $\alpha_k$  and  $S_k$

$$\partial_t \alpha_k + c(x) \partial_x \alpha_k + \lambda \alpha_k = 0, \quad \alpha_k(0, x) = f_k(x), \quad (13a)$$

$$\partial_t S_k + c(x) \partial_x S_k = a(x), \quad S_k(0, x) = k\beta(x). \quad (13b)$$

This gives rise to non oscillatory solutions  $S_k$  and  $\alpha_k$  which can be solved numerically quite efficiently without numerically resolving the small time and wavelength scales of size  $\mathcal{O}(\varepsilon)$ .

### 3.1 Quantum simulation of (13a-13b) with constant convection term

Next we describes the quantum simulation of equation (10). First of all, we consider the case of equations (13a-13b) with  $c(x) \equiv c \neq 0$  and  $c \in \mathbb{R}$ . We choose an uniform mesh size for  $x$  set by  $M_x = 2N_x$ . If not specified, the grid sizes are all indicated by these notations in the rest of this paper. After the Fourier spectral discretisation on  $x$  in (13a), one easily has

$$\frac{d}{dt} \boldsymbol{\alpha}_k + icP_x \boldsymbol{\alpha}_k + \lambda \boldsymbol{\alpha}_k = \mathbf{0}, \quad (14)$$

where  $\boldsymbol{\alpha}_k(t) = \sum_j \alpha_k(t, x_j) |j\rangle$ . Moreover, by denoting  $\mathbf{c}_k = F_x^{-1} \boldsymbol{\alpha}_k(t)$ , one then gets

$$\frac{d}{dt} \mathbf{c}_k + icD_x \mathbf{c}_k + \lambda \mathbf{c}_k = \mathbf{0}.$$

It can also be rewritten as

$$\frac{d}{dt} \mathbf{c}_k = -i(cD_x + \text{Im}(\lambda)I_{M_x}) \mathbf{c}_k - \text{Re}(\lambda)I_{M_x} \mathbf{c}_k.$$

Since the identity matrix is commutative with any matrix, then by using  $\tilde{\mathbf{c}}_k(t) = e^{\text{Re}(\lambda)t} \mathbf{c}_k(t)$ , we can get the following Hamiltonian system:

$$i \frac{d}{dt} \tilde{\mathbf{c}}_k = (cD_x + \text{Im}(\lambda)I_{M_x}) \tilde{\mathbf{c}}_k, \quad \tilde{\mathbf{c}}_k(0) = F_x^{-1} \boldsymbol{\alpha}_k(0).$$

On the other hand, by applying the Fourier transform on  $x$  in (13b), we can get

$$\frac{d}{dt} \mathbf{S}_k + icP_x \mathbf{S}_k = \mathbf{a}, \quad (15)$$

where  $\mathbf{S}_k(t) = \sum_j S_k(t, x_j) |j\rangle$  and  $\mathbf{a} = \sum_j a(x_j) |j\rangle$ . In the same way, let  $\mathbf{d}_k = F_x^{-1} \mathbf{S}_k(t)$  and  $\tilde{\mathbf{a}} = F_x^{-1} \mathbf{a}$ . We then have

$$\frac{d}{dt} \mathbf{d}_k + icD_x \mathbf{d}_k = \tilde{\mathbf{a}}.$$

For this case, we adopt the following approach. By using  $\tilde{\mathbf{d}}_k = cD_x \mathbf{d}_k + i\tilde{\mathbf{a}}$ , we finally get the Hamiltonian system:

$$i \frac{d}{dt} \tilde{\mathbf{d}}_k = cD_x \tilde{\mathbf{d}}_k, \quad \tilde{\mathbf{d}}_k(0) = cD_x F_x^{-1} \mathbf{S}_k(0) + iF_x^{-1} \mathbf{a}.$$

If  $D_x(j, j) = 0$  for (at most) one  $j$ , it means  $\langle j | \frac{d}{dt} \tilde{\mathbf{d}}_k = \langle j | \tilde{\mathbf{a}}$  such that  $\langle j | \tilde{\mathbf{d}}_k$  linearly evolves. So we can just remove it to simulate a  $(M_x - 1)$ -order equation or replace  $D_x(j, j)$  with any non-zero real number. In fact, (14) and (15) correspond to two types of ODEs

$$\frac{d}{dt} x = iHx + \lambda I_n x, \quad \frac{d}{dt} y = iHy + F.$$

where  $\lambda \in \mathbb{C}, x, y, F \in \mathbb{C}^n$  and  $H \in \mathbb{C}^{n \times n}$  is a Hermitian matrix. They can be transformed into Hamiltonian systems by using transformation  $\tilde{x} = e^{-\text{Re}(\lambda)t} x$  (which also can be derived by Corollary 1) and  $\tilde{y} = Hy - iF$  without adding any independent variable. Finally, we denote  $m_x$  to be the number of qubits on  $x$  register and can obtain the following estimation.

**Theorem 3.1.** *For a constant convection term, the solution to the equations (13a) and (13b) can be simulated with gate complexity*

$$N_{\text{Gates}} = \mathcal{O}(m_x \log(m_x)).$$

*Proof.* It is known that the quantum Fourier transforms on  $x$  in one dimension can be implemented using  $\mathcal{O}(m_x \log m_x)$  gates. Moreover, the diagonal unitary operators can be implemented using  $\mathcal{O}(m_x)$  gates. Thus, the proof is completed through Lemma 2.1.  $\square$

## 3.2 Quantum simulation of (13a-13b) with general non-negative convection term

For non-constant convection term  $c(x) \geq 0$ , we cannot get a diagonal unitary operator by the way in section 3.1. We will use the Schrödingerisation approach with a uniform mesh size for  $p$  set by  $M_p = 2N_p$ .



### 3.2.1 Quantum simulation with the spectral method

By applying the Fourier collocation spectral discretisation on  $x$  in (13a) and (13b), we can obtain

$$\frac{d}{dt}\boldsymbol{\alpha}_k + iC(x)P_x\boldsymbol{\alpha}_k + \lambda\boldsymbol{\alpha}_k = \mathbf{0}, \quad (16a)$$

$$\frac{d}{dt}\mathbf{S}_k + iC(x)P_x\mathbf{S}_k = \mathbf{a}, \quad (16b)$$

where  $C(x) = \text{diag}[c(x_0), c(x_1), \dots, c(x_{M_x-1})]$ . Then, applying the Schrödingerisation method in section 2 we can get the following Hamiltonian system from (16a):

$$i\frac{d}{dt}\mathbf{c}_k = (H_1 \otimes D_p - H_2 \otimes I_{M_p})\mathbf{c}_k := H_\alpha\mathbf{c}_k, \quad (17)$$

where  $\mathbf{c}_k(0) = (I_{M_x} \otimes (\Phi_p)^{-1}) \sum_{j,k} \xi(p_k)\alpha_k(0, x_j) |j\rangle |k\rangle$  and

$$H_1 = -\text{Re}(\lambda)I_{M_x} - i\frac{C(x)P_x - P_xC(x)}{2},$$

$$H_2 = -\text{Im}(\lambda)I_{M_x} - \frac{C(x)P_x + P_xC(x)}{2}.$$

On the one hand, one can also obtain the Hamiltonian system from (16b):

$$i\frac{d}{dt}\mathbf{d}_k = (H_1 \otimes D_p - H_2 \otimes I_{M_p})\mathbf{d}_k := H_S\mathbf{d}_k, \quad (18)$$

where  $\mathbf{d}_k(0) = (I_{M_x} \otimes (\Phi_p)^{-1}) \sum_{j,k} \xi(p_k)S_k(0, x_j) |j\rangle |k\rangle$  and

$$H_1 = \frac{1}{2} \begin{bmatrix} i(P_xC(x) - C(x)P_x) & A \\ A & \mathbf{0} \end{bmatrix},$$

$$H_2 = \frac{1}{2i} \begin{bmatrix} -i(C(x)P_x + P_xC(x)) & A \\ -A & \mathbf{0} \end{bmatrix}, \quad A = \text{diag}\{\mathbf{a}\}.$$

It should be mentioned that principal diagonal of  $i(P_xC(x) - C(x)P_x)$  are all zero. Thus, for estimations of the maximal eigenvalue, one can use Gershgorin's Theorem or other effective ways. Then the technique in Corollary 1 can be used by choosing an appropriate  $\lambda_0$ . After the Hamiltonian simulations of (17) and (18),  $\boldsymbol{\alpha}_k(T)$  and  $\mathbf{S}_k(T)$  can be recovered according to (8). In the rest of paper, we won't repeat this explanation again and will point out explicit eigenvalue if it is possible. For a description of Schrödingerisation method, we express the above process by the following Algorithm 1.

We denote  $m_x$  and  $m_p$  to be the number of qubits on  $x$  and  $p$  registers, respectively. The total number of qubits is then given by  $m_H = m_x + m_p$ . Note  $m_x \sim \log 1/\Delta x$  and  $m_p \sim \log 1/\Delta p$  and let  $m = \max\{m_x, m_p\}$ .

**Theorem 3.2.** *The solutions to the equations (16a) and (16b) can be simulated with gate complexity*

$$N_{\text{Gates}} = \mathcal{O}(2^{m_H+1} \frac{m_H^2}{\log m_H}) + \mathcal{O}(m \log m).$$

---

**Algorithm 1**


---

**Input:**  $u_0(x)$

- 1: Give the initial data  $\alpha_k(0, x)$  and  $S_k(0, x)$  according to  $u_0(x)$ .
- 2: Encode initial data into initial states  $|\tilde{\psi}_c(0)\rangle = \frac{\mathbf{c}_k(0)}{\|\mathbf{c}_k(0)\|}, |\tilde{\psi}_d(0)\rangle = \frac{\mathbf{d}_k(0)}{\|\mathbf{d}_k(0)\|}$ .
- 3: Perform Hamiltonian simulation to implement the unitary operators  $e^{-iH_\alpha T}, e^{-iH_S T}$  on initial states to get  $|\tilde{\psi}_c(T)\rangle$  and  $|\tilde{\psi}_d(T)\rangle$ .
- 4: Apply QFT on the resulting state to retrieve  $|\psi_c(T)\rangle$  and  $|\psi_d(T)\rangle$ .
- 5: Conduct measurement in section 2.2 and use (8) to recover the numerical solutions of  $\alpha_k^d(T, x)$  and  $S_k^d(T, x)$ .
- 6: Restore the numerical solution  $u^d(T, x)$  due to the ansatz (12).

**Output:**  $u^d(T, x)$  or other required data

---

*Proof.* By noting that  $s(H_\alpha) = s(H_S) = \mathcal{O}(M_x)$  and  $\|H_\alpha\| = \|H_S\| = \mathcal{O}(M_p)$ , one has

$$\frac{\log(\tau/\delta)}{\log \log(\tau/\delta)} = \mathcal{O}\left(\frac{m_H}{\log m_H}\right).$$

By assuming the regularity in  $p$  of the initial condition implies first-order accuracy on the spatial discretization, the error bound  $\delta = \mathcal{O}(1/2^m)$ . Then we can derive the conclusion according to Lemma 2.1. □

### 3.2.2 Quantum simulation with the finite difference discretisation

On the other hand, one can also apply the finite difference approximation to (13a-13b). For example, if the upwind scheme is used, one gets

$$\begin{aligned} \frac{d\alpha_k^j(t)}{dt} + c(x_j) \frac{\alpha_k^j - \alpha_k^{j-1}}{\Delta x} + \lambda \alpha_k^j &= 0, & \alpha_k^j(0) &= f_k(x_j), \\ \frac{dS_k^j(t)}{dt} + c(x_j) \frac{S_k^j - S_k^{j-1}}{\Delta x} &= a(x_j), & S_k^j(0) &= k\beta(x_j). \end{aligned}$$

An increment operation can be defined as follows:

$$S^+ := \sum_{j=1}^{M_x-1} |j\rangle \langle j-1| = \sum_{j=1}^{m_x} I_{2^{m_x-j}} \otimes \sigma_{10} \otimes \sigma_{01}^{\otimes(j-1)}, \quad S^- = (S^+)^\dagger$$

with  $2 \times 2$  matrices  $\sigma_{ij} = |i\rangle \langle j|$ . Then by denoting  $\boldsymbol{\alpha}_k(t) = \sum_j \alpha_k^j(t) |j\rangle, \mathbf{S}_k = \sum_j S_k^j |j\rangle$  and

$$D_x^- = \frac{1}{\Delta x} (I_{M_x} - S^+ - \sigma_{01}^{\otimes m_x}), \quad D_x^+ = -(D_x^-)^\dagger,$$

we can write the above equation in vector form as

$$\frac{d\boldsymbol{\alpha}_k}{dt} = M_1 \boldsymbol{\alpha}_k \tag{19a}$$

$$\frac{d\mathbf{S}_k}{dt} = M_2 \mathbf{S}_k + F_k, \tag{19b}$$

where  $M_1 = -C(x)D_x^- - \lambda I_{M_x}$ ,  $M_2 = -C(x)D_x^-$  and  $F_k = \sum_j a(x_j) |j\rangle$ . Furthermore, one has

$$\begin{aligned} H_1 &= -\text{Re}(\lambda)I_{M_x} + \frac{D_x^+ C(x) - C(x)D_x^-}{2}, \\ H_2 &= -\text{Im}(\lambda)I_{M_x} - \frac{D_x^+ C(x) + C(x)D_x^-}{2i} \end{aligned}$$

for (19b) while

$$\begin{aligned} H_1 &= \frac{1}{2} \begin{bmatrix} D_x^+ C(x) - C(x)D_x^- & A \\ A & \mathbf{0} \end{bmatrix}, \\ H_2 &= \frac{1}{2i} \begin{bmatrix} -D_x^+ C(x) - C(x)D_x^- & A \\ -A & \mathbf{0} \end{bmatrix}, \quad A = \text{diag}\{F_k\} \end{aligned}$$

for (19b). Then we can obtain the following estimation.

**Theorem 3.3.** *The solutions to the equations (19a-19b) can be simulated with gate complexity*

$$N_{\text{Gates}} = \mathcal{O}\left(2^{m_H} \frac{m_H^2}{\log m_H}\right) + \mathcal{O}(m \log m).$$

*Proof.* It is evident that the sparsity of  $M_i$  is  $\mathcal{O}(1)$  which means  $s(H_i) = \mathcal{O}(1)$ . The norm of  $M_i$  satisfies  $\|M_i\|_\infty = \mathcal{O}(M_x)$  due to the stability condition of the scheme. Then we have  $\|H\|_\infty = \mathcal{O}(M_x M_p)$ . Through calculation we can have

$$\frac{\log(\tau/\delta)}{\log \log(\tau/\delta)} = \mathcal{O}\left(\frac{m_H}{\log m_H}\right).$$

By using Lemma 2.1, we can finish the proof.  $\square$

### 3.3 Numerical results

Next we will present some tests to ensure the effectiveness of our quantum algorithms. In this paper, the Hamiltonian simulation is implemented by the implicit midpoint rule which is also a symplectic method of order 2. In addition, we use (5) for initializations. Furthermore, we denote  $M_x = 2^m$  and  $M_p = 2^n$  in this section for later use.

#### 3.3.1 A constant convection term case

First we consider a constant convection case for benchmark with  $c(x) = \lambda = a(x) = 1$  and the following initial data

$$u_0(x) = 1 + \frac{1}{2} \cos(2x) + i\left(1 + \frac{1}{2} \sin(2x)\right), \quad x \in \left[-\frac{\pi}{2}, \frac{\pi}{2}\right]. \quad (20)$$

The periodic boundary condition is chosen such that the exact solution is given by  $u(t, x) = \exp(-(1 - i/\varepsilon)t)u_0(x - t)$ . Figure 1 shows the comparison between the exact solution and the numerical solution for different values of  $\varepsilon$  at the final time  $T = 1$ . It can be observed that the numerical solutions match the accurate solutions well on all three scales.

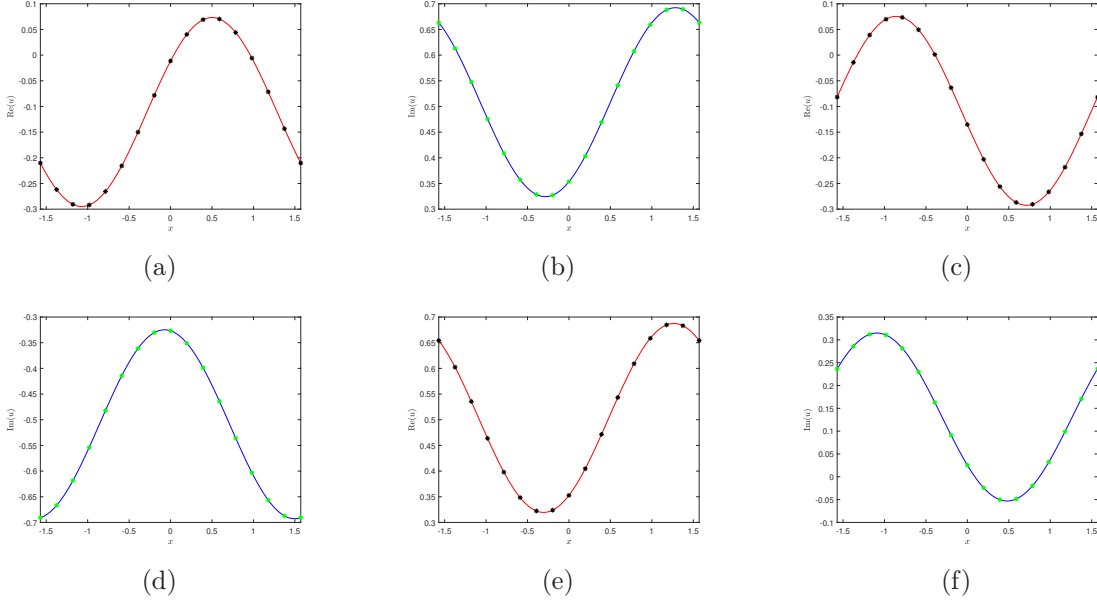


Figure 1: Comparison between the exact solution and the numerical solution for  $T = 1, m = 4$ . (a)(c)(e): Real part of  $u$ . (b)(d)(f): Imaginary part of  $u$ . (a)(b):  $\varepsilon = 1$ . (c)(d):  $\varepsilon = 0.1$ . (e)(f):  $\varepsilon = 0.01$ .

To further display the capability of numerical method for capturing oscillations generated from both initial data and source—even without numerically resolving the oscillations, we add an oscillatory dependence with the initial phase  $x/\varepsilon$  in Figure 2. The exact solution under periodic boundary condition and initial data

$$u_0(x) = e^{i\frac{x}{\varepsilon}} \left( 1 + \frac{1}{2} \cos(2x) + i \left( 1 + \frac{1}{2} \sin(2x) \right) \right), \quad x \in \left[ -\frac{\pi}{2}, \frac{\pi}{2} \right].$$

is given by  $\exp(-t + ix/\varepsilon)u_0(x - t)$ . Since  $\alpha_k$  and  $S_k$  are not oscillatory, they can be solved quite efficiently by our algorithm.

### 3.3.2 A general nonnegative convection term case

In this test, we solve (10) with  $c(x) = \cos^2(x), a(x) = 1.5 + \cos(2x)$  with the initial data (20) at the final time  $T = 1$ , and mesh size  $m = 5, n = 9$ . For this case, the Schrödingerisation method in section 3.2 should be applied. Since the spectral method and finite difference method have almost no different on performance in Figure 3, we just plot one of them and illustrate the space-time oscillations arising in the solution with  $a(x)$ . We can observe that our method is able to capture very well high oscillations, *point-wise*, in space—even without numerically resolving the oscillations, whether  $S_k$  is accurately solved or not.

In Figure 4 and Figure 5, we plot the error  $\|\alpha_k^d(T, x) - \alpha_k(T, x)\|_\infty$  obtained by different recoveries. The error is computed at the final time  $T = 1$  by mesh size  $m = 4, n = 9$ . We choose  $\lambda_0 \in [-6 - \lambda, 6 - \lambda]$  while the computational domain of  $p$  is  $[-10, 10]$  due to  $\lambda_n(H_1) = 113/30 - \lambda$  and  $\lambda_1(H_1) = -113/30 - \lambda$ . And in Figure 6, we plot the bar graph of the number  $\text{card}(\{p_j : \|\alpha_k^d(T, x, p_j) - \alpha_k(T, x)\|_\infty \leq \Delta p\})$

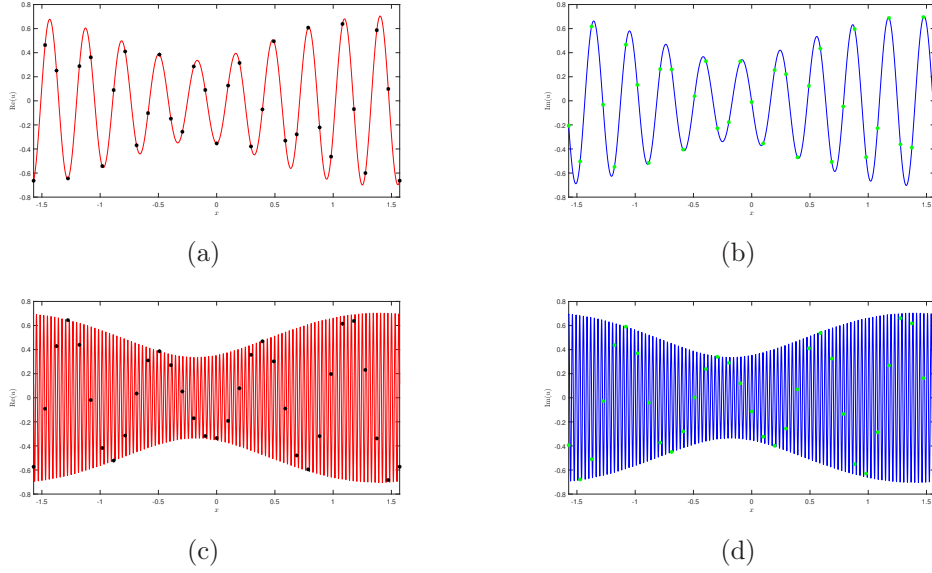


Figure 2: Comparison between the exact solution and the numerical solution for  $T = 1, m = 5$ . (a)(c): Real part of  $u$ . (b)(d): Imaginary part of  $u$ . (a)(b):  $\varepsilon = 0.1$ . (c)(d):  $\varepsilon = 0.01$ .

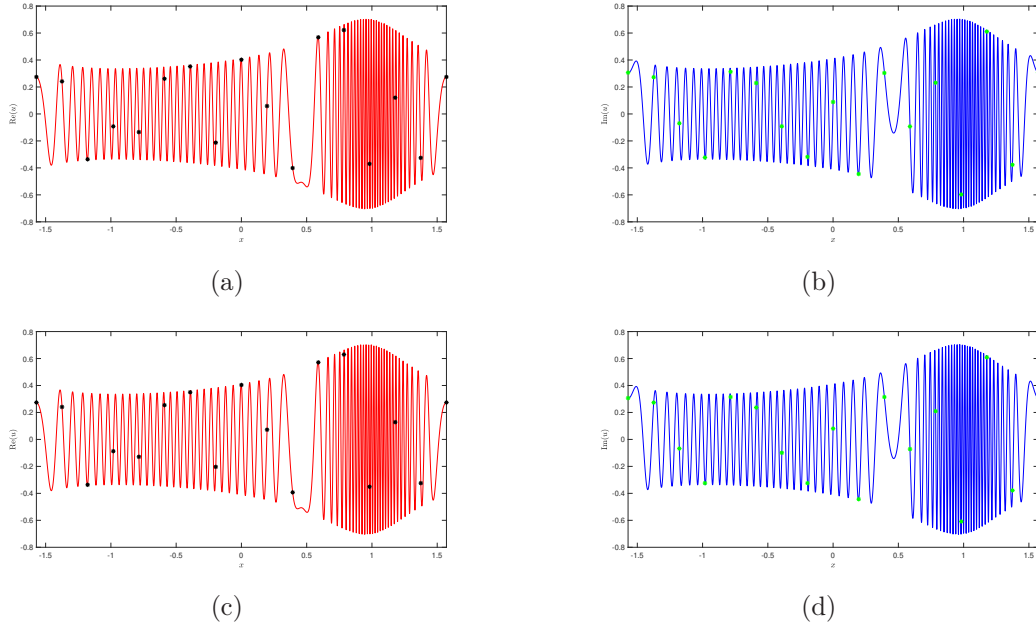


Figure 3: Comparison between the exact solution and the solution of algorithm 1 for  $\varepsilon = 0.01, T = 1, m = 4, n = 9, \lambda = 1$ . (a)(b): Numerical computation for  $S_k$ . (c)(d): Exact computation for  $S_k$ . (a)(c): Real part of  $u$ . (b)(d): Imaginary part of  $u$ .

for various  $\lambda$  and  $\lambda_0$ . It can be observed that the optimal recovery of Schrödingerisation can be obtained by choosing a certain  $\lambda_0$  which belongs to  $[\frac{\lambda_1(H_1) + \lambda_n(H_1)}{2}, \lambda_n(H_1)]$ .

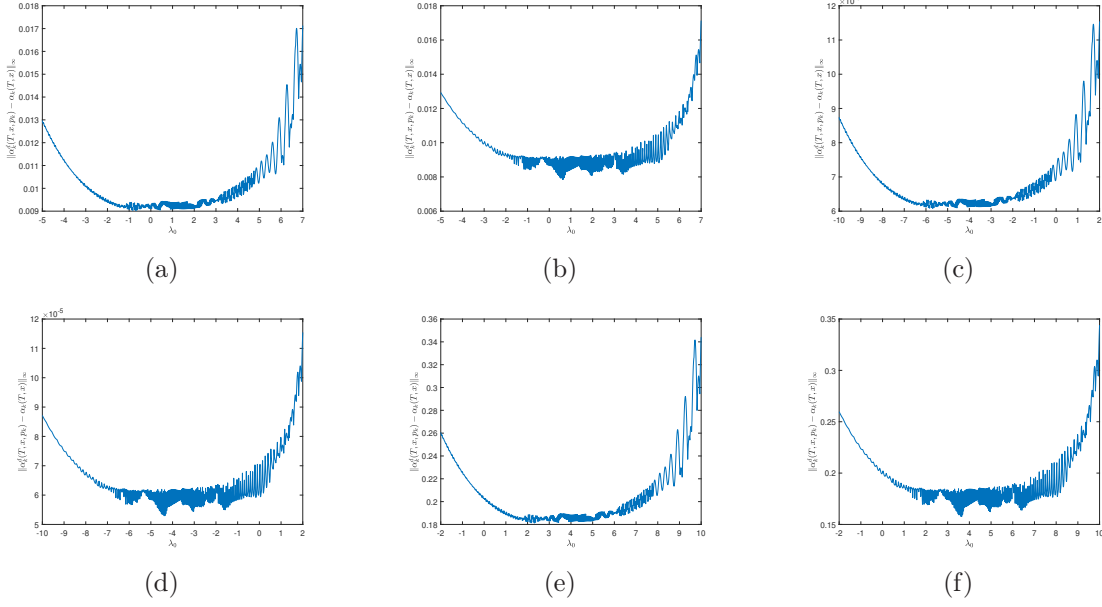


Figure 4: Plot of the error estimation  $\|\alpha_k^d(T, x, p_k) - \alpha_k(T, x)\|_\infty$  for  $T = 1, m = 4, n = 9$ . (a)(c)(e):  $p_k = \min\{p_j : p_j \geq p_\star\}$ . (b)(d)(f):  $p_k = \arg \min_{p_j} \|\alpha_k^d(T, x, p_j) - \alpha_k(T, x)\|_\infty$ . (a)(b):  $\lambda = -1$ . (c)(d):  $\lambda = 4$ . (e)(f):  $\lambda = -4$ .

## 4 Extension to a class of PDE systems

In this section, we will focus on the case where  $u(t, x) \in \mathbb{C}^2, x \in [0, 1], t \geq 0$ ,

$$\partial_t u + A(x)\partial_x u = \frac{iE(t, x)}{\varepsilon} Du + Cu, \quad u(0, x) = u_0(x). \quad (21)$$

$E$  is a real scalar function,  $C$  is a constant matrix and

$$A(x) = \begin{bmatrix} a_1(x) & 0 \\ 0 & a_2(x) \end{bmatrix}, \quad D = \begin{bmatrix} 0 & 0 \\ 0 & -1 \end{bmatrix}, \quad C = \begin{bmatrix} C_{11} & C_{12} \\ C_{21} & C_{22} \end{bmatrix}.$$

To construct the uniformly accurate numerical scheme in [11], we use the nonlinear geometric optics (NGO) ansatz:

$$U(t, x, S(t, x)/\varepsilon) = u(t, x).$$

Then,  $U = (U_1, U_2)$  satisfies

$$\begin{aligned} \partial_t U_1 + a_1 \partial_x U_1 + \frac{1}{\varepsilon} [\partial_t S + a_1 \partial_x S] \partial_\tau U_1 &= C_{11} U_1 + C_{12} U_2, \\ \partial_t U_2 + a_2 \partial_x U_2 + \frac{1}{\varepsilon} [\partial_t S + a_2 \partial_x S] \partial_\tau U_2 &= -\frac{iE}{\varepsilon} U_2 + C_{21} U_1 + C_{22} U_2. \end{aligned}$$

The equation for the phase  $S$  writes

$$\partial_t S + a_2 \partial_x S = E, \quad S(0, x) = 0, \quad (22)$$

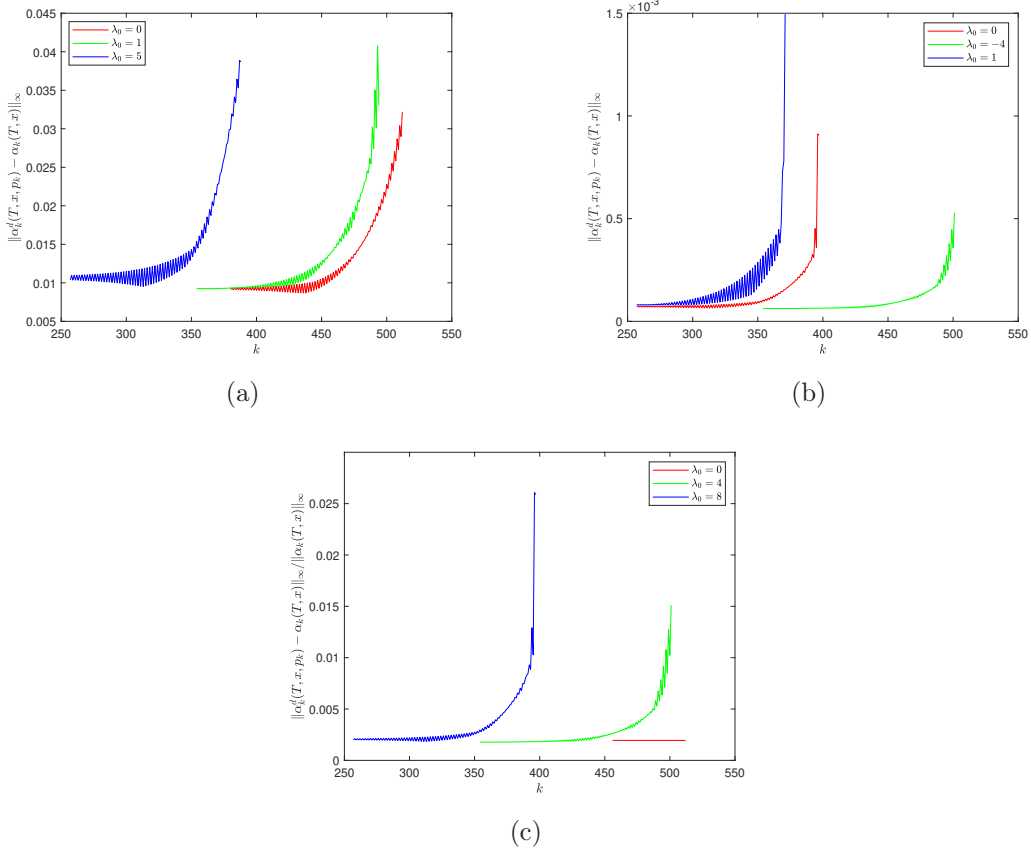


Figure 5: Plot of the error estimation  $\|\alpha_k^d(T, x, p_k) - \alpha_k(T, x)\|_\infty$  for  $T = 1, m = 4, n = 9$ . (a):  $\lambda = -1$  and  $p_k \in \{p_j : \|\alpha_k^d(T, x, p_j) - \alpha_k(T, x)\|_\infty \leq \Delta p\}$ . (b):  $\lambda = 4$  and  $p_k \in \{p_j : \|\alpha_k^d(T, x, p_j) - \alpha_k(T, x)\|_\infty \leq \Delta p^2\}$ . (c):  $\lambda = -4$  and  $p_k \in \{p_j : \|\alpha_k^d(T, x, p_j) - \alpha_k(T, x)\|_\infty \leq \Delta p \|\alpha_k(T, x)\|_\infty\}$ .

and the equations for  $(U_1, U_2)$  become

$$\begin{aligned} \partial_t U_1 + a_1 \partial_x U_1 + \frac{1}{\varepsilon} [(a_1 - a_2) \partial_x S + E] \partial_\tau U_1 &= C_{11} U_1 + C_{12} U_2, \\ \partial_t U_2 + a_2 \partial_x U_2 &= -\frac{E}{\varepsilon} [\partial_\tau U_2 + i U_2] + C_{21} U_1 + C_{22} U_2. \end{aligned}$$

Setting  $V_2 = e^{i\tau} U_2$ , we finally obtain

$$\begin{aligned} \partial_t U_1 + a_1 \partial_x U_1 - C_{11} U_1 - C_{12} e^{-i\tau} V_2 &= -\frac{1}{\varepsilon} [(a_1 - a_2) \partial_x S + E] \partial_\tau U_1, \\ \partial_t V_2 + a_2 \partial_x V_2 - C_{21} e^{i\tau} U_1 - C_{22} V_2 &= -\frac{E}{\varepsilon} \partial_\tau V_2. \end{aligned} \tag{23}$$

Also, (23) needs appropriate initial data  $U_1(0, x, \tau)$  and  $V_2(0, x, \tau)$ . A suitable initial condition with first order correction for them is provided using the Chapman-

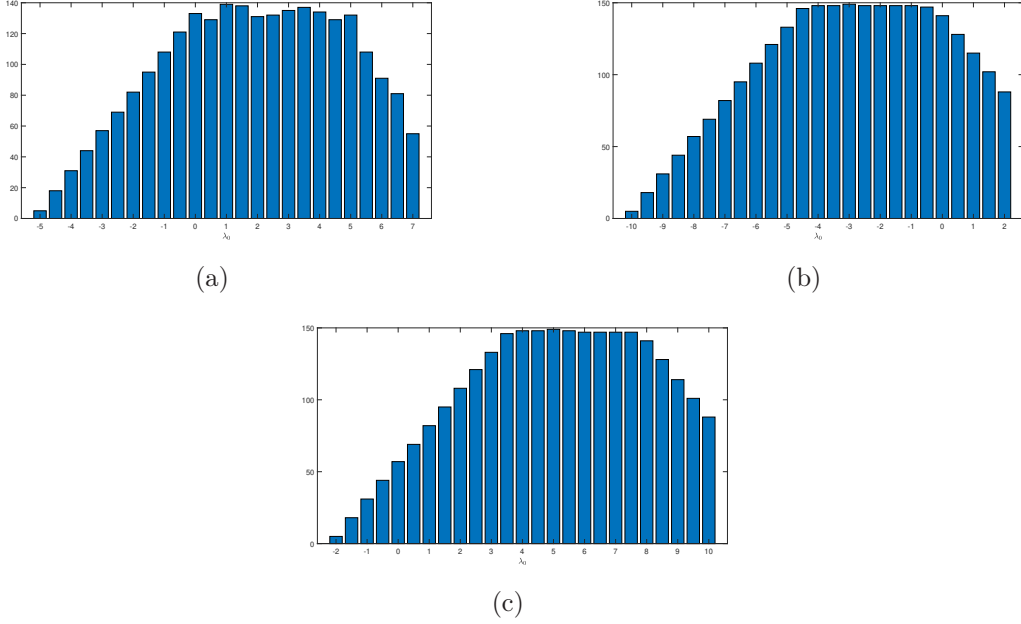


Figure 6: Plot of the number  $card(\{p_j : \|\alpha_k^d(T, x, p_j) - \alpha_k(T, x)\|_\infty \leq tol\})$  for  $T = 1, m = 4, n = 9$ . (a):  $\lambda = -1, tol = \Delta p$ . (b):  $\lambda = 4, tol = \Delta p^2$ . (c):  $\lambda = -4, tol = \Delta p \|\alpha_k(T, x)\|_\infty$ .

Enskog expansion [11], and is given by

$$\begin{aligned}
 U_1(0, x, \tau) &= f_1^{in} + \frac{i\varepsilon EC_{12}}{E^2 - \varepsilon^2 C_{12} C_{21}} (e^{-i\tau} - 1) f_2^{in} \\
 U_2(0, x, \tau) &= \frac{i\varepsilon EC_{21}}{E^2 - \varepsilon^2 C_{12} C_{21}} (e^{-i\tau} - 1) f_1^{in} + e^{-i\tau} f_2^{in},
 \end{aligned} \tag{24}$$

where  $u_0(x) = U(0, x, 0) = (f_1^{in}(x), f_2^{in}(x))^T$ .

## 4.1 Quantum simulation of system (23)

In this section, we consider the quantum algorithm to solve (23). Since the phase  $S$  in (22) can be solved as in section 3, we will omit the detailed computation for it and suppose it has been well approximated.

### 4.1.1 Quantum simulation with the spectral method

By applying the Fourier spectral discretisation on  $x$  and  $\tau$  in (23), we can get

$$\partial_t \mathbf{u} + i(A_1 P_x) \otimes I_{M_\tau} \mathbf{u} - C_{11} \mathbf{u} - C_{12} T_1 \mathbf{v} = \frac{1}{\varepsilon} \text{diag} \{(A_1 - A_2) P_x \mathbf{S} - i\mathbf{E}\} \otimes P_\tau \mathbf{u}, \tag{25a}$$

$$\partial_t \mathbf{v} + i(A_2 P_x) \otimes I_{M_\tau} \mathbf{v} - C_{21} T_2 \mathbf{u} - C_{22} \mathbf{v} = -\frac{i}{\varepsilon} \text{diag} \{\mathbf{E}\} \otimes P_\tau \mathbf{v}, \tag{25b}$$

$$\partial_t \mathbf{S} + iA_2 P_x \mathbf{S} = \mathbf{E}, \tag{25c}$$



where  $\mathbf{u} = \sum_{j,k} U_1(t, x_j, \tau_k) |j\rangle |k\rangle$ ,  $\mathbf{v} = \sum_{j,k} V_2(t, x_j, \tau_k) |j\rangle |k\rangle$  and  $\mathbf{S} = \sum_j S(t, x_j) |j\rangle$ . The matrices  $A_1, A_2, \mathbf{E}$  and  $T_1, T_2$  are defined by

$$A_1 = \text{diag} \left\{ \sum_j a_1(x_j) |j\rangle \right\}, A_2 = \text{diag} \left\{ \sum_j a_2(x_j) |j\rangle \right\}, \mathbf{E} = \sum_j E(x_j) |j\rangle,$$

$$T_1 = I_{M_x} \otimes \text{diag} \left\{ \sum_k e^{-i\tau_k} |k\rangle \right\}, T_2 = I_{M_x} \otimes \text{diag} \left\{ \sum_k e^{i\tau_k} |k\rangle \right\} = T_1^\dagger.$$

Then we can further write Equation (25a-25b) in vector form as  $\dot{\mathbf{z}} = M\mathbf{z}$  where  $\mathbf{z} = [\mathbf{u}; \mathbf{v}]$  and

$$\begin{aligned} M = & \sigma_{00} \otimes (-i(A_1 P_x) \otimes I_{M_\tau} + C_{11} I_{M_x} \otimes I_{M_\tau} + \frac{1}{\varepsilon} \text{diag} \{ (A_1 - A_2) P_x \mathbf{S} - i\mathbf{E} \} \otimes P_\tau) \\ & + \sigma_{11} \otimes (-i(A_2 P_x) \otimes I_{M_\tau} + C_{22} I_{M_x} \otimes I_{M_\tau} - \frac{i}{\varepsilon} \text{diag} \{ \mathbf{E} \} \otimes P_\tau) \\ & + C_{12} \sigma_{01} \otimes T_1 + C_{21} \sigma_{10} \otimes T_2. \end{aligned}$$

Moreover, we can find

$$\begin{aligned} H_1 = & \sigma_{00} \otimes \left( \text{Re}(C_{11}) I_{M_x} \otimes I_{M_\tau} - \frac{iA_1 P_x - iP_x A_1}{2} \otimes I_{M_\tau} \right) \\ & + \sigma_{11} \otimes \left( \text{Re}(C_{22}) I_{M_x} \otimes I_{M_\tau} - \frac{iA_2 P_x - iP_x A_2}{2} \otimes I_{M_\tau} \right) \\ & + \frac{C_{12} + \overline{C_{21}}}{2} \sigma_{01} \otimes T_1 + \frac{\overline{C_{12}} + C_{21}}{2} \sigma_{10} \otimes T_2, \end{aligned}$$

and

$$\begin{aligned} H_2 = & \sigma_{00} \otimes \left( \text{Im}(C_{11}) I_{M_x} \otimes I_{M_\tau} - \frac{A_1 P_x + P_x A_1}{2} \otimes I_{M_\tau} - \frac{1}{\varepsilon} \text{diag} \{ i(A_1 - A_2) P_x \mathbf{S} + \mathbf{E} \} \otimes P_\tau \right) \\ & + \sigma_{11} \otimes \left( \text{Im}(C_{22}) I_{M_x} \otimes I_{M_\tau} - \frac{A_2 P_x + P_x A_2}{2} \otimes I_{M_\tau} - \frac{1}{\varepsilon} \text{diag} \{ \mathbf{E} \} \otimes P_\tau \right) \\ & + i \frac{\overline{C_{21}} - C_{12}}{2} \sigma_{01} \otimes T_1 + i \frac{\overline{C_{12}} - C_{21}}{2} \sigma_{10} \otimes T_2. \end{aligned}$$

Then the homogeneous system can be solved by Schrödingerisation with a well approximated  $\mathbf{S}$ . Since the corresponding Hermitian matrix of  $M$  is time-dependent, strategy in section 2.3 can be taken. On the other hand, Schrödingerisation can also be used for  $\mathbf{S}$  via (25c). When  $A_1, A_2$  are both constant matrices, it's easy to check that

$$\lambda(H_1) = \frac{\text{Re}(C_{11} + C_{22}) + \sqrt{(\text{Re}(C_{11} - C_{22}))^2 + |C_{12} + \overline{C_{21}}|^2}}{2}$$

so that  $H_1$  will be a zero matrix, i.e.  $M = iH_2$  if  $\text{Re}(C_{11}) = \text{Re}(C_{22}) = C_{12} + \overline{C_{21}} = 0$ . Thus, in this case the warped phase transformation is not needed for  $\mathbf{z}$ .

We denote by  $m_\tau$  the number of qubits in  $\tau$  and then the total number of qubits is given by  $m_H = m_x + m_\tau + m_p$ . In addition,  $m$  represents the maximum value of  $\{m_x, m_\tau, m_p\}$ .

**Theorem 4.1.** *If  $\|E\|_\infty = \mathcal{O}(1)$ , the solutions to the equations (25a-25b) can be simulated with gate complexity*

$$N_{\text{Gates}} = \mathcal{O}\left(9 \cdot 2^{2m+1} \frac{m^2}{\log m}\right) + \mathcal{O}(m \log m).$$

*Proof.* After a direct calculation, we have  $s(H) = s(M) = M_x + M_\tau$  and  $\|H\|_\infty = \mathcal{O}(M_p)$ . The rest of the proof is similar to that in Theorem 3.3, so we omit it here.  $\square$

#### 4.1.2 Quantum simulation with the finite difference discretisation

By denoting  $U_{j,k}(t) \approx U_1(t, x_j, \tau_k)$  and  $V_{j,k} \approx V_2(t, x_j, \tau_k)$ , the approximations to (23) can be obtained by the following upwind numerical scheme

$$\begin{aligned} & \frac{dU_{j,k}}{dt} + a_1(x_j) \frac{U_{j,k} - U_{j-1,k}}{\Delta x} - C_{11}U_{j,k} - C_{12}e^{-i\tau_k}V_{j,k} \\ &= -\frac{1}{\varepsilon} (E_j + (a_1(x_j) - a_2(x_j))\partial_x S(x_j)) \frac{U_{j,k} - U_{j,k-1}}{\Delta \tau}, \\ & \frac{dV_{j,k}}{dt} + a_2(x_j) \frac{V_{j,k} - V_{j-1,k}}{\Delta x} - C_{21}e^{i\tau_k}U_{j,k} - C_{22}V_{j,k} \\ &= -\frac{1}{\varepsilon} E_j \frac{V_{j,k} - V_{j,k-1}}{\Delta \tau}, \end{aligned} \tag{26}$$

where  $E_j = E(t, x_j)$ . Certainly, high-order methods should be used for the approximation of  $S$ . By further denoting  $\mathbf{u}(t) = \sum_{j,k} U_{j,k}(t) |j\rangle |k\rangle$ ,  $\mathbf{v}(t) = \sum_{j,k} V_{j,k}(t) |j\rangle |k\rangle$  and  $\mathbf{z} = [\mathbf{u}; \mathbf{v}]$ , the above scheme can be written in vector form as  $\dot{\mathbf{z}} = M\mathbf{z}$  where

$$\begin{aligned} M &= \sigma_{00} \otimes (-(A_1 D_x^-) \otimes I_{M_\tau} + C_{11} I_{M_x} \otimes I_{M_\tau} - \frac{1}{\varepsilon} \text{diag}\{\mathbf{E} + (A_1 - A_2)\partial_x \mathbf{S}\} \otimes D_\tau^-) \\ &+ \sigma_{11} \otimes (-(A_2 D_x^-) \otimes I_{M_\tau} + C_{22} I_{M_x} \otimes I_{M_\tau} - \frac{1}{\varepsilon} \text{diag}\{\mathbf{E}\} \otimes D_\tau^-) \\ &+ C_{12}\sigma_{01} \otimes T_1 + C_{21}\sigma_{10} \otimes T_2. \end{aligned}$$

Meanwhile, we can get

$$\begin{aligned} H_1 &= \sigma_{00} \otimes \left( \left( \frac{D_x^+ A_1 - A_1 D_x^-}{2} \right) \otimes I_{M_\tau} + C_{11} I_{M_x} \otimes I_{M_\tau} + \frac{1}{\varepsilon} \text{diag}\{\mathbf{E} + (A_1 - A_2)\partial_x \mathbf{S}\} \otimes \frac{D_\tau^+ - D_\tau^-}{2} \right) \\ &+ \sigma_{11} \otimes \left( \left( \frac{D_x^+ A_2 - A_2 D_x^-}{2} \right) \otimes I_{M_\tau} + C_{22} I_{M_x} \otimes I_{M_\tau} + \frac{1}{\varepsilon} \text{diag}\{\mathbf{E}\} \otimes \frac{D_\tau^+ - D_\tau^-}{2} \right) \\ &+ \frac{C_{12} + C_{21}}{2} \sigma_{01} \otimes T_1 + \frac{C_{12} + C_{21}}{2} \sigma_{10} \otimes T_2, \end{aligned}$$

and

$$\begin{aligned} H_2 &= i\sigma_{00} \otimes \left( \left( \frac{D_x^+ A_1 + A_1 D_x^-}{2} \right) \otimes I_{M_\tau} + \frac{1}{\varepsilon} \text{diag}\{\mathbf{E} + (A_1 - A_2)\partial_x \mathbf{S}\} \otimes \frac{D_\tau^+ + D_\tau^-}{2} \right) \\ &+ i\sigma_{11} \otimes \left( \left( \frac{D_x^+ A_2 + A_2 D_x^-}{2} \right) \otimes I_{M_\tau} + \frac{1}{\varepsilon} \text{diag}\{\mathbf{E}\} \otimes \frac{D_\tau^+ + D_\tau^-}{2} \right) \\ &+ i\frac{C_{21} - C_{12}}{2} \sigma_{01} \otimes T_1 + i\frac{C_{12} - C_{21}}{2} \sigma_{10} \otimes T_2. \end{aligned}$$

## 4.2 Numerical results

In this section, we will present the numerical experiments for the new approach. The parameters in (21) are chosen as  $a_1(x) = 1, a_2(x) = 4, E(t, x) = 1.5 + \cos(x)$ , and

$$C = \begin{bmatrix} 0 & 1 \\ -1 & 0 \end{bmatrix}.$$

The initial condition is

$$u(0, x) = \left( 1 + \frac{1}{2} \cos(x) + i \sin(x), 1 + \frac{1}{2} \cos(x) + i \sin(x) \right), \quad x \in [0, 2\pi].$$

In the following figures, we compare a reference solution (computed with time splitting method with resolved numerical computation) and the solution of our quantum algorithm with the corrected initial condition (24). For the reference solution, we set the cell number as  $M_x = 2^8$ .

In Figure 7, we plot the real and imaginary part of components of the solution as a function of space for final time  $T = 1$ . We can observe that the our method is able to capture the high space oscillations of the solution with a spatial mesh independent of  $\varepsilon$ .

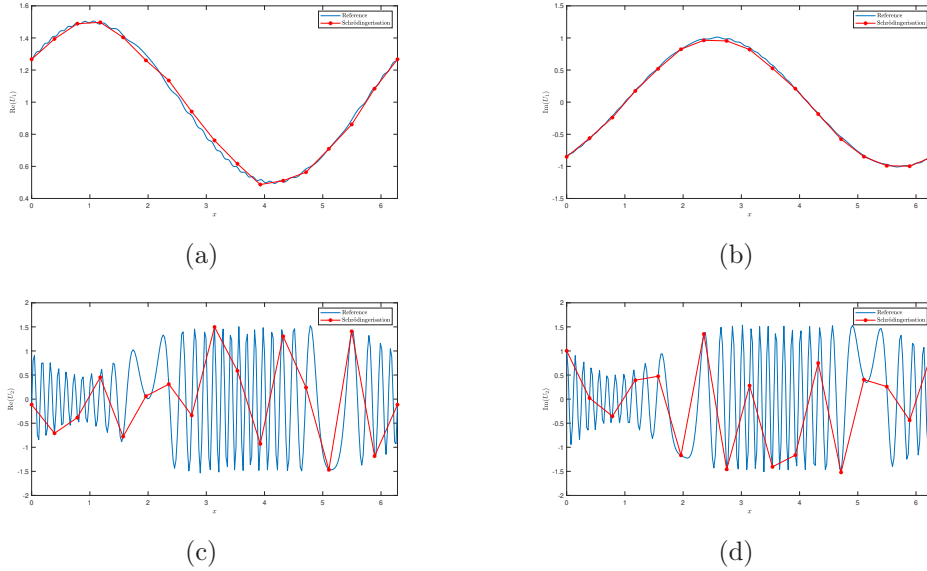


Figure 7: Comparison between the reference solution and the numerical solution (with exact solution for  $S$ ) for  $\varepsilon = 0.1, T = 1, l = 3, m = 4$ . (a), (b):  $U_1$ . (c), (d):  $U_2$ .

Then, we illustrate the performances of the Schrödingerisation method by using the same data as before except the constant matrix

$$C = \frac{1}{2} \begin{bmatrix} 1+i & 1+i \\ -1+i & 1-i \end{bmatrix}.$$

The computational domain of  $p$  is  $[-5, 5]$ . According to Corollary 1, we choose  $\lambda_0 = \frac{T}{2}$  and non-negative  $p_k$  to recover the solution  $\mathbf{z}$ . As shown in Figure 8, the Schrödingerisation method captures the high space oscillations of the solution,

point-wise, well even if the spatial mesh  $\Delta x = \frac{2\pi}{24}$  is large compared to the size of the oscillation ( $\varepsilon = 0.01$ ).

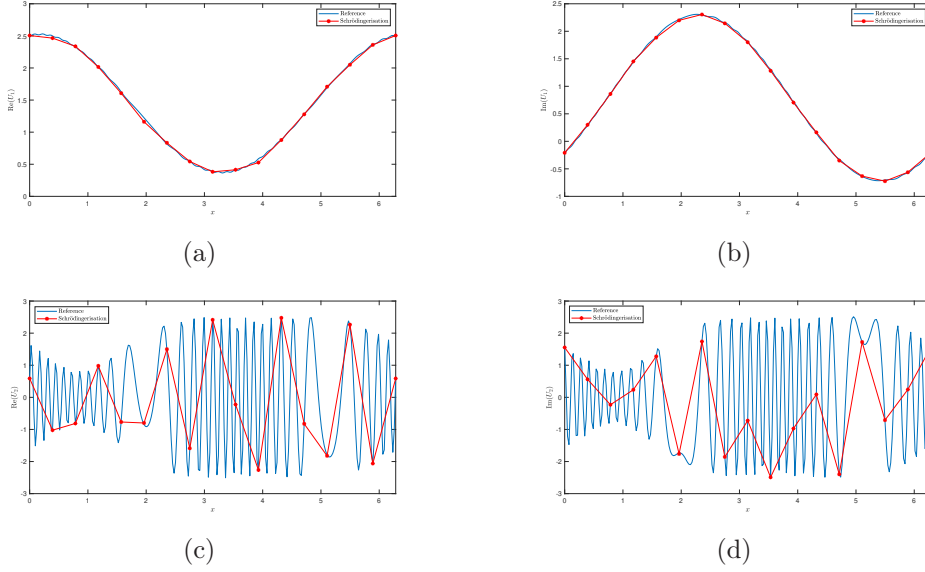


Figure 8: Comparison between the reference solution and the numerical solution of Schrödingerisation (with exact solution for  $S$ ) for  $\varepsilon = 0.01, T = 1, l = 3, m = 4, n = 8$ . (a):  $U_1$ . (b):  $U_2$ .

### 4.3 Quantum simulation for the surface hopping model

Finally, we show that the general quantum approach described above can be extended to efficiently solve the following semiclassical surface hopping model. This model approximates semiclassically the nucleonic Schrödinger system arising from the Born-Oppenheimer approximation with non-adiabatic corrections. For more details see [7]. Specifically, this model can be expressed as the following equations,

$$\begin{aligned}
\partial_t f^+ + v \cdot \nabla_x f^+ - \nabla_x(U + E) \cdot \nabla_v f^+ &= \bar{b}^i f^i + b^i \bar{f}^i, \\
\partial_t f^- + v \cdot \nabla_x f^- - \nabla_x(U - E) \cdot \nabla_v f^- &= -\bar{b}^i f^i - b^i \bar{f}^i, \\
\partial_t f^i + v \cdot \nabla_x f^i - \nabla_x U \cdot \nabla_v f^i &= -i \frac{2E}{\varepsilon} f^i + b^i (f^- - f^+) + (b^+ - b^-) f^i,
\end{aligned} \tag{27}$$

where  $(f^+(t, x, v), f^-(t, x, v), f^i(t, x, v)) \in \mathbb{R} \times \mathbb{R} \times \mathbb{C}$ ,  $(t, x, v) \in \mathbb{R}_+ \times \mathbb{R}^d \times \mathbb{R}^d$ , and  $b^\pm, \bar{b}^i \in \mathbb{C}, U, E \in \mathbb{R}$  are given functions depending only on the space variable  $x$ . The initial conditions are denoted by

$$(f^+(0, x, v), f^-(0, x, v), f^i(0, x, v)) = (f_{in}^+(x, v), f_{in}^-(x, v), f_{in}^i(x, v)).$$

In vector form, (27) becomes

$$\partial_t \mathbf{f} + \mathbf{v} \cdot \nabla_x \mathbf{f} - \nabla_x A \cdot \nabla_v \mathbf{f} = C \mathbf{f}, \tag{28}$$

where

$$\mathbf{f} = (f^+, f^-, \text{Re}(f^i), \text{Im}(f^i))^T, \quad \mathbf{v} = (v, v, v, v)^T, \quad A = \text{diag}(U + E, U - E, U, U),$$

$$C = \begin{bmatrix} 0 & 0 & b^i + \bar{b}^i & -ib^i + i\bar{b}^i \\ 0 & 0 & -b^i - \bar{b}^i & ib^i - i\bar{b}^i \\ -b^i & b^i & b^+ - b^- & 2E/\varepsilon \\ 0 & 0 & -2E/\varepsilon & b^+ - b^- \end{bmatrix}.$$

A direct time splitting scheme for (28) writes

- solve  $\partial_t \mathbf{f} + \mathbf{v} \cdot \nabla_x \mathbf{f} = 0$  by spectral method in space and exact integration in time,
- solve  $\partial_t \mathbf{f} - \nabla_x A \cdot \nabla_v \mathbf{f} = 0$  by spectral method in velocity and exact integration in time,
- solve  $\partial_t \mathbf{f} = C \mathbf{f}$  by exact integration.

For an explanation of quantum simulation on (28), we consider  $b^i \in \mathbb{R}, b^\pm = 0$  which corresponds to two potential matrices introduced in [7]. By introducing a phase  $S(t, x, v)$ , solution to

$$\partial_t S + v \cdot \nabla_x S - \nabla_x U \cdot \nabla_v S = 2E, \quad S(0, x, v) = 0, \quad (29)$$

and the augmented unknowns  $(F^\pm, F^i)(t, x, v, \tau)$  with  $\tau = S(t, x, v)/\varepsilon$  satisfying

$$f^\pm(t, x, v) = F^\pm(t, x, v, \tau), \quad f^i(t, x, v) = e^{-i\tau}(G + iH)(t, x, v, \tau),$$

where  $G = \text{Re}(e^{i\tau} f^i), H = \text{Im}(e^{i\tau} f^i)$ . Then it has

$$\begin{aligned} \partial_t F^+ + v \cdot \nabla_x F^+ - \nabla_x(U + E) \cdot \nabla_v F^+ &= -\frac{\mathcal{E}^+}{\varepsilon} \partial_\tau F^+ + 2b^i G \cos \tau + 2b^i H \sin \tau, \\ \partial_t F^- + v \cdot \nabla_x F^- - \nabla_x(U - E) \cdot \nabla_v F^- &= -\frac{\mathcal{E}^-}{\varepsilon} \partial_\tau F^- - 2b^i G \cos \tau - 2b^i H \sin \tau, \\ \partial_t G + v \cdot \nabla_x G - \nabla_x U \cdot \nabla_v G &= -\frac{2E}{\varepsilon} \partial_\tau G + b^i(F^- - F^+) \cos \tau, \\ \partial_t H + v \cdot \nabla_x H - \nabla_x U \cdot \nabla_v H &= -\frac{2E}{\varepsilon} \partial_\tau H + b^i(F^- - F^+) \sin \tau, \end{aligned} \quad (30)$$

where  $\mathcal{E}^\pm = 2E \mp \nabla_x E \cdot \nabla_v S$ . The initial data can be derived from the Chapman-Enskog expansion which yields

$$\begin{aligned} F^+(0, x, v, \tau) &= f_{in}^+ - i\frac{\varepsilon}{2E} \left( b^i f_{in}^i (1 - e^{-i\tau}) - b^i \overline{f_{in}^i} (1 - e^{i\tau}) \right), \\ F^-(0, x, v, \tau) &= f_{in}^- + i\frac{\varepsilon}{2E} \left( b^i f_{in}^i (1 - e^{-i\tau}) - b^i \overline{f_{in}^i} (1 - e^{i\tau}) \right), \\ G(0, x, v, \tau) &= \text{Re}(f_{in}^i) - \frac{\varepsilon}{2E} b^i (f_{in}^+ - f_{in}^-) \sin \tau, \\ H(0, x, v, \tau) &= \text{Im}(f_{in}^i) + \frac{\varepsilon}{2E} b^i (f_{in}^+ - f_{in}^-) (\cos \tau - 1). \end{aligned} \quad (31)$$

Then we apply the Schrödingerisation method for (30) with initial data (31). Without loss of generality, we set  $d = 1$ . By denoting  $\mathbf{g} = (F^+, F^-, G, H)^T$ , (30) becomes the following vector form

$$\partial_t \mathbf{g} + v \partial_x \mathbf{g} + A \partial_v \mathbf{g} + B \partial_\tau \mathbf{g} = C \mathbf{g}, \quad (32)$$

where

$$A = \partial_x \text{diag}(-U - E, -U + E, -U, -U), \quad B = \text{diag}\left(\frac{\mathcal{E}^+}{\varepsilon}, \frac{\mathcal{E}^-}{\varepsilon}, \frac{2E}{\varepsilon}, \frac{2E}{\varepsilon}\right),$$

$$C = \begin{bmatrix} 0 & 0 & 2b^i \cos \tau & 2b^i \sin \tau \\ 0 & 0 & -2b^i \cos \tau & -2b^i \sin \tau \\ -b^i \cos \tau & b^i \cos \tau & 0 & 0 \\ -b^i \sin \tau & b^i \sin \tau & 0 & 0 \end{bmatrix}.$$

By applying the Fourier spectral discretisation on  $x, v, \tau$  in (32), we can get

$$\begin{aligned} \frac{d}{dt} \tilde{\mathbf{g}} &= (-i(P_x \otimes I_4 \otimes \text{diag}\{\sum_j v_j |j\rangle\}) \otimes I_{M_\tau} + \sum_i |i\rangle \langle i| \otimes A(x_i) \otimes P_v \otimes I_{M_\tau} \\ &+ \sum_{i,j} |i\rangle \langle i| \otimes B(t, x_i, v_j) \otimes I_{M_v} \otimes P_\tau) + \sum_{i,j,k} |i\rangle \langle i| \otimes |j\rangle \langle j| \otimes |k\rangle \langle k| \otimes C(x_i, v_j, \tau_k)) \tilde{\mathbf{g}}, \end{aligned} \quad (33)$$

where  $\tilde{\mathbf{g}} = \sum_{i,j,k} \mathbf{g}(t, x_i, v_j, \tau_k) |i\rangle |j\rangle |k\rangle$ . One can further get

$$H_1 = \sum_{i,j,k} |i\rangle \langle i| \otimes |j\rangle \langle j| \otimes |k\rangle \langle k| \otimes \frac{C(x_i, v_j, \tau_k) + C^T(x_i, v_j, \tau_k)}{2}$$

and

$$\begin{aligned} H_2 &= -(P_x \otimes I_4 \otimes \text{diag}\{\sum_j v_j |j\rangle\}) \otimes I_{M_\tau} + \sum_i |i\rangle \langle i| \otimes A(x_i) \otimes P_\tau \otimes I_{M_\tau} \\ &+ \sum_i |i\rangle \langle i| \otimes B(x_i) \otimes I_{M_v} \otimes P_\tau \\ &- i \sum_{i,j,k} |i\rangle \langle i| \otimes |j\rangle \langle j| \otimes |k\rangle \langle k| \otimes \frac{C(x_i, v_j, \tau_k) - C^T(x_i, v_j, \tau_k)}{2}. \end{aligned}$$

And one can further get  $\lambda_n(H_1) = \frac{\|b^i\|_\infty}{\sqrt{2}}$ .

## 4.4 Numerical results

This section is devoted to the numerical experiments of the Schrödingerisation approach for the surface hopping model. We consider the following initial conditions with  $x, v \in [-2\pi, 2\pi]$

$$\begin{aligned} f^+(0, x, v) &= f^-(0, x, v) = \left(1 + \frac{1}{2} \cos(x)\right) \frac{e^{-v^2/2}}{\sqrt{2\pi}}, \\ f^i(0, x, v) &= f^-(0, x, v) = \left(\left(1 + \frac{1}{2} \sin(x)\right) + i \left(1 + \frac{1}{2} \cos(x)\right)\right) \frac{e^{-v^2/2}}{\sqrt{2\pi}}, \end{aligned}$$

and functions

$$U(x) = 0, \quad E(x) = 1 - \cos(x/2) + \varepsilon, \quad b^i(x, v) = -\frac{1}{2} \sin(v + 1), \quad b^\pm = 0.$$

For all the following tests, the reference solution is computed by the time splitting method. Moreover, we use notations  $M_\tau = 2^k, M_v = 2^l, M_x = 2^m, M_p = 2^n$  for the cell number of the Schrödingerisation method in this section. Since we don't perform the experiments on a quantum computer now, the huge cost for solving

(33) directly by Schrödingerisation in classic computer is unacceptable. Thus, in the practical simulation we consider a further splitting for (33). Furthermore, we choose  $[-5, 5]$  for the computational region of  $p$ .

In Figure 9, we plot the solutions  $f^{\pm,i}(T, x, v)$  and densities  $\rho^{\pm,i}(T, x, v) = \int_{-2\pi}^{2\pi} f^{\pm,i}(T, x, v) dp$  for two methods. The reference solution is computed by using  $\Delta t = 0.005, M_v = 2^4, M_x = 2^6$ . For  $\varepsilon = 1$ , the densities evolve without oscillations. And it can be observed that our method matches well, point-wise, the solutions and densities.

In Figure 10, we show the densities  $\rho^{\pm,i}(T, x, v)$  for two methods. The reference solution is calculated by using  $\Delta t = 10^{-5}, M_v = 2^6, M_x = 2^8$ . Numerical solution is computed by Schrödingerisation with the corrected initial data (31) and recovered by using  $\lambda_0 = \frac{\sqrt{2}}{4}$  and non-negative  $p_k$  according to Corollary 1. In this instance, the densities are highly oscillatory due to  $\varepsilon \ll 1$ . However, our method captures very well, point-wise, all densities, even though the mesh is much coarser than the spatial oscillations.

## 5 Conclusion

In this paper, we proposed quantum algorithms for the following highly-oscillatory transport equations

$$\partial_t u + \sum_{k=1}^d A_k(x) \partial_{x_k} u = \frac{iE(t, x)}{\varepsilon} Du + Cu$$

by using the Schrödingerisation approach introduced in [26, 27] combined with the nonlinear geometric optics (NGO) method [11]. About the Schrödingerisation method, we also illustrate the influence of shifting the eigenvalues of linear systems' Hermite parts depending on whether they contain unstable modes or not. This technique can help the recoveries of the original problem, and will be further studied in our following work.

Such numerical methods allow us to obtain accurate numerical solutions, in maximum norm, with mesh size *independent* of the wave length. Our approach can be further extended to higher dimensional problems which is no longer suitable for classical computing. This is also why we need to design quantum algorithms for these equations. Numerical examples demonstrate that the proposed method has the desired property of capturing the pointwise solutions of highly oscillatory waves with mesh sizes independent of the wave length.

In our future work, we will design detailed quantum circuits of this method, which is important for future qubit-based general purpose quantum computers.

## Acknowledgement

The research results of this article are sponsored by the Kunshan Municipal Government research funding.

## References

- [1] Dong An, Di Fang, and Lin Lin. Time-dependent unbounded Hamiltonian simulation with vector norm scaling. *Quantum*, 5:459, May 2021.
- [2] Dong An, Di Fang, and Lin Lin. Time-dependent Hamiltonian Simulation of Highly Oscillatory Dynamics and Superconvergence for Schrödinger Equation. *Quantum*, 6:690, Apr 2022.
- [3] Dominic W Berry. High-order quantum algorithm for solving linear differential equations. *Journal of Physics A: Mathematical and Theoretical*, 47(10):105301, feb 2014.
- [4] Dominic W. Berry, Andrew M. Childs, and Robin Kothari. Hamiltonian simulation with nearly optimal dependence on all parameters. In *2015 IEEE 56th Annual Symposium on Foundations of Computer Science*, pages 792–809, 2015.
- [5] Dominic W. Berry, Andrew M. Childs, Yuan Su, Xin Wang, and Nathan Wiebe. Time-dependent Hamiltonian simulation with  $L^1$ -norm scaling. *Quantum*, 4:254, Apr 2020.
- [6] Yu Cao, Shi Jin, and Nana Liu. Quantum simulation for time-dependent Hamiltonians – with applications to non-autonomous ordinary and partial differential equations, 2023.
- [7] Lihui Chai, Shi Jin, Qin Li, and Omar Morandi. A multiband semiclassical model for surface hopping quantum dynamics. *Multiscale Modeling & Simulation*, 13(1):205–230, 2015.
- [8] Andrew M. Childs and Jin-Peng Liu. Quantum spectral methods for differential equations. *Communications in Mathematical Physics*, 375:1427–1457, 2020.
- [9] Andrew M. Childs, Jin-Peng Liu, and Aaron Ostrander. High-precision quantum algorithms for partial differential equations. *Quantum*, 5:574, November 2021.
- [10] Pedro C. S. Costa, Stephen Jordan, and Aaron Ostrander. Quantum algorithm for simulating the wave equation. *Phys. Rev. A*, 99:012323, Jan 2019.
- [11] Nicolas Crouseilles, Shi Jin, and Mohammed Lemou. Nonlinear geometric optics method-based multi-scale numerical schemes for a class of highly oscillatory transport equations. *Mathematical Models and Methods in Applied Sciences*, 27(11):2031–2070, 2017.
- [12] David Deutsch. Quantum theory, the church–turing principle and the universal quantum computer. *Proceedings of the Royal Society of London. A. Mathematical and Physical Sciences*, 400(1818):97–117, 1985.
- [13] David P DiVincenzo. Quantum computation. *Science*, 270(5234):255–261, 1995.
- [14] Artur Ekert and Richard Jozsa. Quantum algorithms: entanglement–enhanced information processing. *Philosophical Transactions of the Royal Society of London. Series A: Mathematical, Physical and Engineering Sciences*, 356(1743):1769–1782, 1998.



- [15] Alexander Engel, Graeme Smith, and Scott E. Parker. Quantum algorithm for the vlasov equation. *Phys. Rev. A*, 100:062315, Dec 2019.
- [16] Di Fang, Lin Lin, and Yu Tong. Time-marching based quantum solvers for time-dependent linear differential equations. *Quantum*, 7:955, Mar 2023.
- [17] E. Fatemi, B. Engquist, and S. Osher. Numerical solution of the high frequency asymptotic expansion for the scalar wave equation. *Journal of Computational Physics*, 120(1):145–155, 1995.
- [18] Richard P. Feynman. Simulating physics with computers. *International Journal of Theoretical Physics*, 21:467–488, 1982.
- [19] M. Freiser and P. Marcus. A survey of some physical limitations on computer elements. *IEEE Transactions on Magnetism*, 5(2):82–90, 1969.
- [20] Aram W. Harrow, Avinandan Hassidim, and Seth Lloyd. Quantum algorithm for linear systems of equations. *Phys. Rev. Lett.*, 103:150502, Oct 2009.
- [21] Shi Jin, Xiantao Li, Nana Liu, and Yue Yu. Quantum simulation for partial differential equations with physical boundary or interface conditions. *Journal of Computational Physics*, 498:112707, 2024.
- [22] Shi Jin and Nana Liu. Analog quantum simulation of partial differential equations, 2023.
- [23] Shi Jin, Nana Liu, Xiantao Li, and Yue Yu. Quantum simulation for quantum dynamics with artificial boundary conditions, 2023.
- [24] Shi Jin, Nana Liu, and Chuwen Ma. On schrödingerization based quantum algorithms for linear dynamical systems with inhomogeneous terms, 2024.
- [25] Shi Jin, Nana Liu, and Chuwen Ma. Schrödingerisation based computationally stable algorithms for ill-posed problems in partial differential equations, 2024.
- [26] Shi Jin, Nana Liu, and Yue Yu. Quantum simulation of partial differential equations via schrödingerisation, 2022.
- [27] Shi Jin, Nana Liu, and Yue Yu. Quantum simulation of partial differential equations: Applications and detailed analysis. *Phys. Rev. A*, 108:032603, Sep 2023.
- [28] Victor P Maslov and Mikhail Vasilevich Fedoriuk. *Semi-classical approximation in quantum mechanics*, volume 7. Springer Science & Business Media, 2001.
- [29] Ashley Montanaro and Sam Pallister. Quantum algorithms and the finite element method. *Phys. Rev. A*, 93:032324, Mar 2016.
- [30] Omar Morandi. Multiband wigner-function formalism applied to the Zener band transition in a semiconductor. *Phys. Rev. B*, 80:024301, Jul 2009.
- [31] Omar Morandi and Ferdinand Schuerrer. Wigner model for quantum transport in graphene. *Journal of Physics A: Mathematical and Theoretical*, 44:265301, 2011.
- [32] Michael A. Nielsen and Isaac L. Chuang. *Quantum Computation and Quantum Information: 10th Anniversary Edition*. Cambridge University Press, 2010.

- [33] P.W. Shor. Algorithms for quantum computation: discrete logarithms and factoring. In *Proceedings 35th Annual Symposium on Foundations of Computer Science*, pages 124–134, 1994.
- [34] Andrew Steane. Quantum computing. *Reports on Progress in Physics*, 61(2):117, feb 1998.

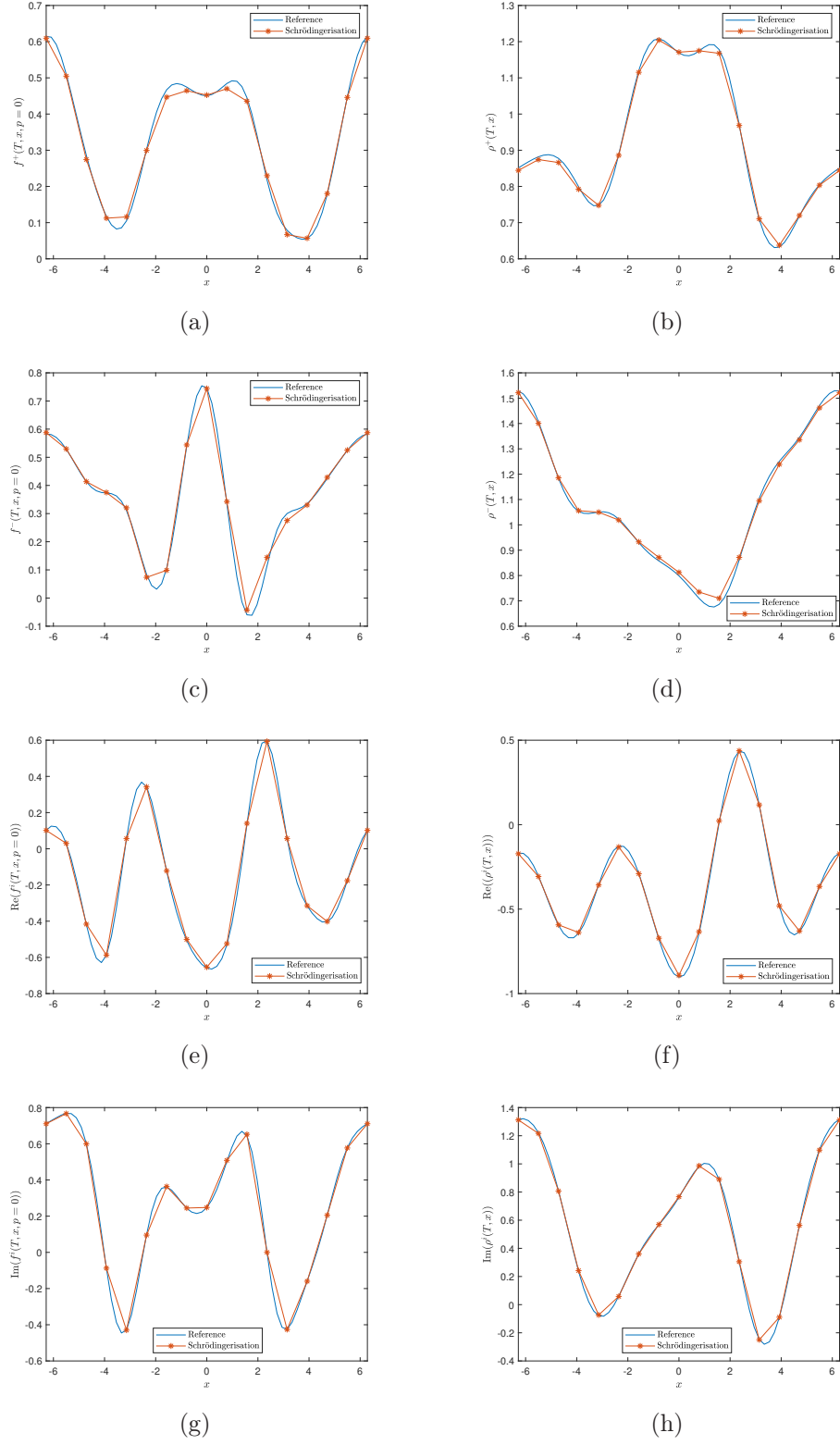


Figure 9: Comparison between a reference solution and the numerical solution of Schrödingerisation (with exact computation for  $S$ ) for  $\varepsilon = 1, T = 2, k = 3, l = 4, m = 4, n = 7$ .

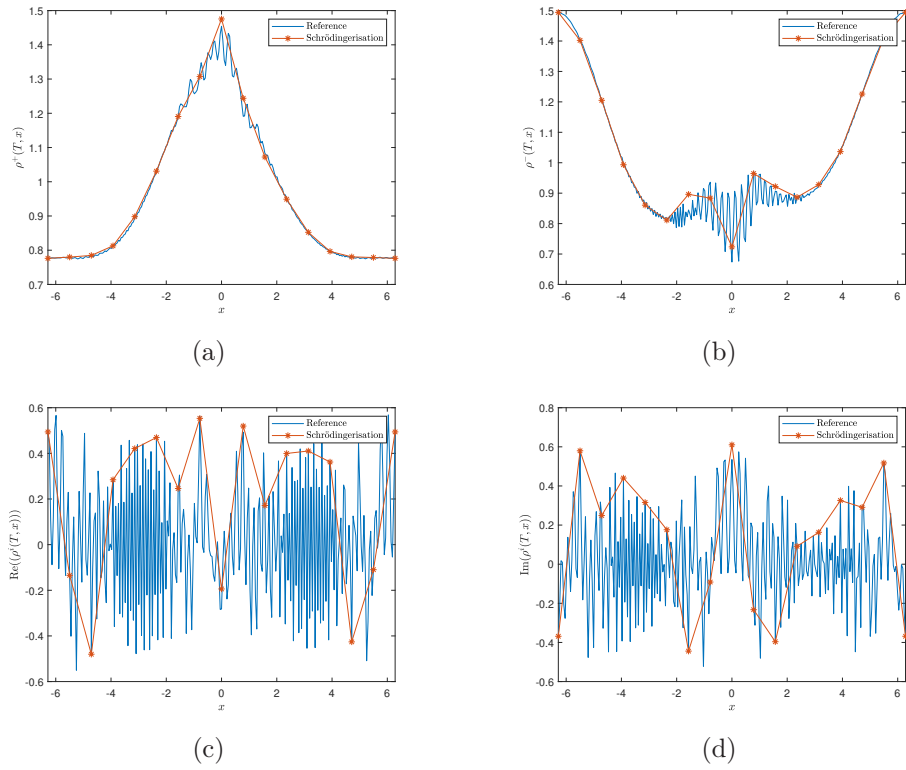


Figure 10: Comparison between a reference solution and the solution of Schrödingerisation (with exact computation for  $S$ ) for  $\varepsilon = 1/32, T = 2, k = 3, l = 6, m = 4, n = 8$ .